Rotational suppression of Rayleigh–Taylor instability

By G. F. CARNEVALE[1], P. ORLANDI[2],
YE ZHOU[3] AND R. C. KLOOSTERZIEL[4]

[1]Scripps Institution of Oceanography, University of California, San Diego, La Jolla,
CA 92093-0225, USA

[2]Dipartimento di Meccanica e Aeronautica, University of Rome, 'La Sapienza',
via Eudossiana 18, 00184 Roma, Italy

[3]University of California, Lawrence Livermore National Laboratory, P.O. Box 808, Livermore,
CA 94551, USA

[4]School of Ocean & Earth Science & Technology, University of Hawaii, Honolulu,
HI 96822, USA

It is demonstrated that the growth of the mixing zone generated by Rayleigh–Taylor instability can be greatly retarded by the application of rotation, at least for low Atwood number flows for which the Boussinesq approximation is valid. This result is analysed in terms of the effect of the Coriolis force on the vortex rings that propel the bubbles of fluid in the mixing zone.

1. Introduction

Rayleigh–Taylor instability (RTI) results from the application of a pressure gradient in the direction opposite to a density gradient. If the variation of density in the fluid is not great, then the development of the instability occurs with the penetration of 'bubbles' of higher density fluid into lower density fluid and vice versa. Visualised with density isosurfaces, these bubbles appear as roughly spherical caps on mushroom-shaped density intrusions. Three-dimensional images of these bubbles can be found in a number of articles (cf. Linden, Redondo & Youngs 1994). The evolution and interaction of numerous bubbles produces a mixing zone. If the advance of those bubbles could be retarded or, better, if they could be kept from forming, then the effects of RTI would be diminished.

A vortex ring is associated with each bubble. To a large extent, these rings determine the evolution of the density intrusions (cf. Zabusky 1999). One way to hinder the development and propagation of the bubbles is to destabilize the vortex rings that drive them. In previous work on unstratified flow, we have shown that vortex rings can be disrupted or prevented from forming if rotation is applied in a direction aligned with the axis of the ring. We demonstrated this in both laboratory experiments and matching numerical simulations (Verzicco *et al.* 1996). These results suggest that it may be possible to slow or even eliminate RTI by the application of ambient rotation. A similar effect would be that of flow curvature. Indeed, Sen & Storer (1997) found that flow curvature can reduce the growth rate of RTI.

RTI is of interest in a wide variety of fields including geophysics, astrophysics, engineering and plasma physics. Specific areas of relevance include mantle convection, deep convection in the oceans, mixing during density overturns in the atmosphere

and oceans, and the design of devices for controlled nuclear fusion. We do not have space here to review the literature. However, we note that for exponentially stratified viscous fluid, without diffusion, Hide (1956) showed with a normal modes analysis that rotation decreases the maximum growth rate of the instability. But rotation could not suppress it completely. We are not aware of similar studies that include the effect of diffusion, but it seems likely that this addition will permit complete suppression.

Here we present the results of a series of numerical simulations demonstrating that, indeed, ambient rotation suppresses RTI. In §3, for cases with random initial perturbations, we show that RTI can be delayed and its growth rate diminished by rotation. Interestingly, we find that the effects of rotation occur even in the earliest phase of the instability, that is even before the establishment of a mixing zone. This suggests that it would be possible to understand the effect of rotation, at least in the early phases, in terms of bubble formation. In Verzicco *et al.* (1996), our understanding of the role of rotation on vortex dynamics came from a focus on the late time evolution of the vortex ring in the rotating environment. There the focus was on the interaction between the primary ring and secondary vorticity structures. This interaction increased the radius of the ring and allowed cross-diffusion between vortex structures. Both of these effects were shown to slow the advance of a vortex ring. In contrast, here in §4, we analyse the retarding role that rotation plays in the early formation of the vortex ring. Further, we find that for high enough rotation rate bubble formation is completely suppressed.

2. Numerical method and unperturbed background

Our experiments are on the incompressible Boussinesq equations using a finite-difference staggered-mesh code with third-order Runge–Kutta time stepping. The details of the numerical methods employed are explained at length in Orlandi (2000). The computational domain is a cube, with vertical z-axis aligned along the direction of gravity ($-g\hat{z}$) and the angular rotation vector ($\Omega\hat{z}$). The horizontal (x, y) boundary conditions are periodic and at the bottom and top there are rigid free-slip boundaries. The unperturbed density profile is explicitly

$$\bar{\rho}(z) = \rho_1 + (\rho_2 - \rho_1)(1 + \tanh(z/l))/2, \tag{2.1}$$

with l fixed as $L/80$ where L is half of the domain height and $\rho_1 < \rho_2$. The code provides more resolution in the region of the density gradient by using a stretched grid in the z-direction (see Orlandi 2000, p. 13, equation 2.24, for clustering near $z = 0$ with the stretching coefficient $a = 1.5$). Except where noted otherwise, the number of grid points in both horizontal periodic directions is 128, and in the vertical 193. The effect of the resolution on the results was checked by comparisons with simulations of resolution $97 \times 97 \times 129$, which showed no significant differences. All of the results presented here are in non-dimensional units with length scaled by L (the vertical and horizontal coordinates run from -1 to 1), velocity scaled by $V_g = \sqrt{2LgA}$ where A is the Atwood number given by $A = (\rho_2 - \rho_1)/(\rho_2 + \rho_1)$, and time by $T = L/V_g$. To ensure the validity of the Boussinesq approximation, the Atwood number is assumed to be small. We will report the density ρ in terms of a scaled variable θ that varies between 0 and 1:

$$\theta = (\rho - \rho_1)/(\rho_2 - \rho_1). \tag{2.2}$$

An important non-dimensional quantity for this study is the Rossby number $Ro = V_g/fL$, where $f = 2\Omega$. For all of the simulations presented here, the Reynolds number,
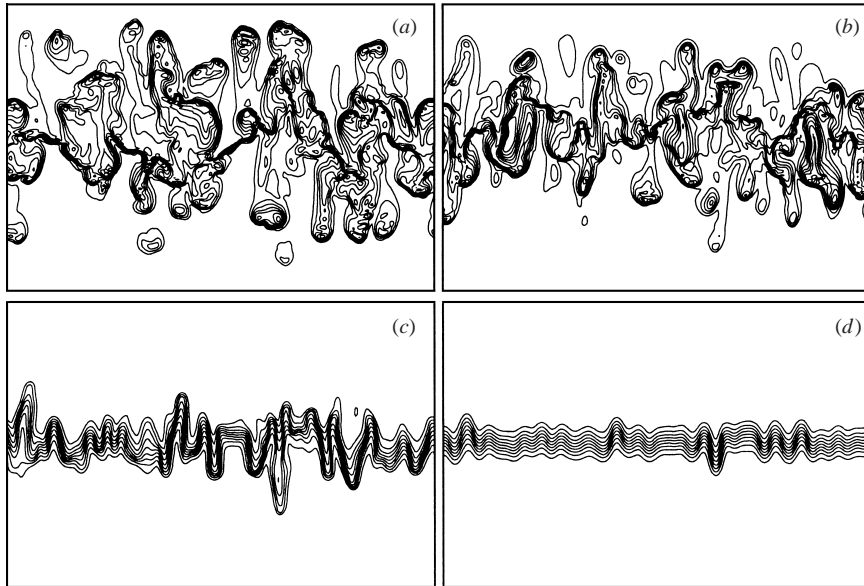
FIGURE 1. Contour plots of the scaled density θ in a vertical cross-section (y,z-plane) at time $t = 5$. The contour increment is $\Delta\theta = 0.1$. Both the vertical axis z and the horizontal axis y range from -1 to 1 (images have been cropped in the vertical direction). (*a*) $Ro = \infty$, (*b*) $Ro = 1/4$, (*c*) $Ro = 1/8$, (*d*) $Ro = 1/12$.

which we define as $Re = LV_g/\nu$, is 5000. We assume a single species flow with a Prandtl number $\nu/\kappa = 1$, where ν is the kinematic viscosity and κ the diffusivity, both assumed constant.

3. Rotational suppression of the growth of the mixing zone

The first simulations that we will present are designed to demonstrate the degree to which rotation delays RTI. Four simulations are presented with $Ro = \infty$, 1/4, 1/8 and 1/12 (where $Ro = \infty$ implies no rotation). In each case, the initial condition was a state of no motion. The initial density field was as described above plus uniformly distributed random noise on each grid point in the range $-0.05 < z < 0.05$ with an r.m.s. level of 9% of the mean density. Figure 1 illustrates the efficacy of rotation in damping the growth of the turbulent mixing zone; it is a vertical cross-section of the three-dimensional density field at time $t = 5$. Panel (*a*) shows the extent and nature of the mixing zone with no rotation. It shows a well-developed turbulent mixed zone with many well-formed mushroom-shaped bubbles and elements of high/low-density fluid that have been carried into the regions of low/high density. Similarly for (*b*) except that with $Ro = 1/4$, the development of the mixing zone has not proceeded as far. As illustrated in panel (*c*), with $Ro = 1/8$, no convincing mixing zone has been established by $t = 5$; there are no fully developed bubbles, and the vertical extent of the perturbations is much reduced compared to that in (*a*) and (*b*). Finally in (*d*) we see that the effect of rotation with $Ro = 1/12$ has diminished the growth of the perturbation so significantly that there is little that can yet be identified as bubble formation.

To further quantify the effect of rotation on slowing the growth of the mixing zone, we have computed an average profile $\bar{\theta}(z,t)$ of the density field by performing a
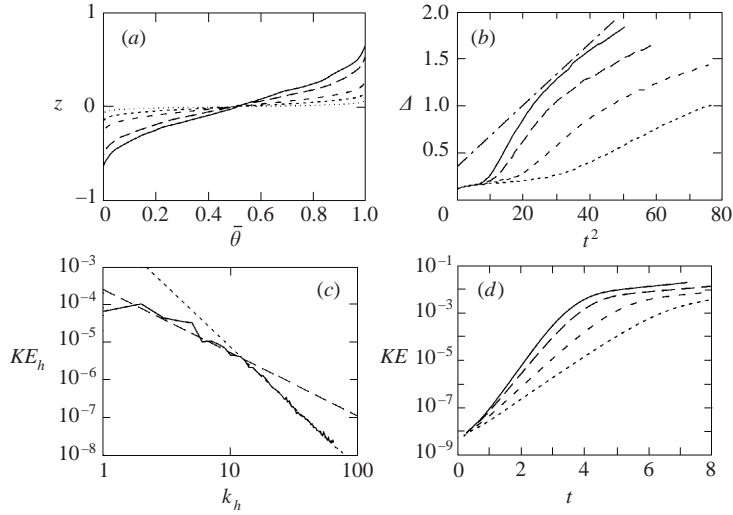
FIGURE 2. (*a*) Profile of $\bar{\theta}$, the horizontally averaged θ, vs. z at time $t = 5$. Dotted line, initial condition; solid, $Ro = \infty$; long dashed, $Ro = 1/4$; dashed, $Ro = 1/8$; short dashed, $Ro = 1/12$. (*b*) Thickness of the mixing zone vs. t^2. The line types are as in (*a*) with an additional line (chain-dashed) representing the similarity solution with slope 0.033 (see text). (*c*) Horizontal kinetic energy spectrum as a function of horizontal wavenumber $k_h = \sqrt{k_x^2 + k_y^2}$ at $t = 10$ for $Ro = \infty$. The long and short dashed straight lines are graphs of $k^{-5/3}$ and $k^{-3.2}$ respectively. (*d*) Total kinetic energy KE vs. time (line types as in *a*).

horizontal average for each z. The result at $t = 5$ is shown in figure 2(*a*) for four values of Ro. During the evolution, a thickness Δ of the mixing zone can be computed by calculating these profiles and then measuring the distance between two density values near the extremes of the density field. We considered the evolution of the vertical distance Δ between $\bar{\theta} = 0.02$ and 0.98. If the flow is sufficiently turbulent so that the details of the initial conditions are irrelevant, then one expects similarity scaling such that $\Delta = \alpha t^2$, where α is a constant to be determined empirically (cf. Linden *et al.* 1994). For comparison with previous work, we plot Δ versus t^2 in figure 2(*b*). For each Ro, we observe a period of slow growth at first that can be understood as simple diffusive spreading of the density gradient. This is followed by a period of rapid growth once the instability begins. With decreasing Ro, the time of onset of instability increases and the maximum growth rate decreases. At late times, particularly in the cases $Ro = \infty$ and 1/4, the growth rate decreases noticeably near the end of the runs because the evolution is affected by the finite domain size. According to Linden *et al.* (1994) the period of t^2 scaling should occur after the initial rapid rise in Δ. In a simulation of their laboratory experiment, they found a slope $\alpha = 0.033$. In our figure, we have added a straight line with that slope. This helps to indicate that for the $Ro = \infty$ case that there is a period of such scaling.

In this study the influence of the top and bottom boundaries is not a primary concern. Rather, we are interested in the development of the instability before saturation effects become apparent. To test the influence of the location of the boundaries, we repeated the simulation for $Ro = \infty$ in a domain of double the vertical extent, also increasing to 256 the number of grid points in the vertical. The evolution of the mixing zone was essentially the same as shown above, except in that the appearance of saturation effects was delayed. In addition, we compared both free-slip and no-
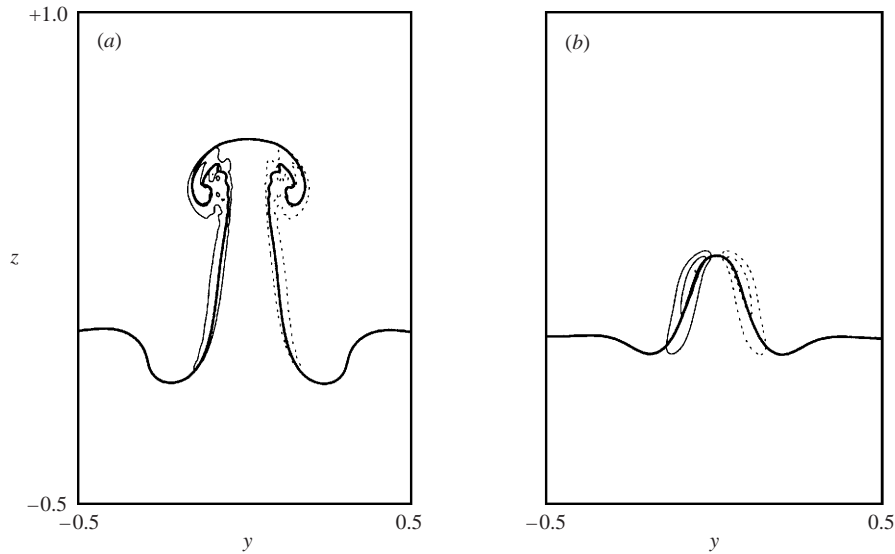
FIGURE 3. Isolated bubble and associated vorticity component ω_x in a y, z cross-section through the centre ($x = 0$) of the bubble at $t = 4$. The thick line is the $\theta = 0.5$ contour. The thin solid/dashed lines are contours of positive/negative ω_x. Only a portion of the computational domain is shown. (a) $Ro = \infty$, vorticity contour interval 7.5, (b) $Ro = 1/4$, contour interval 2.5.

slip boundary conditions and found no significant effect during the time of the rapid growth of the instability. In figure 2(c), we show the horizontal kinetic energy spectrum computed in a horizontal cross-section in the middle of the mixing zone (i.e. at $z = 0$) at $t = 10$ for $Ro = \infty$ for the case with double the vertical size and free-slip boundaries. For large scales, it appears that $-5/3$ scaling holds with a $k^{-3.2}$ fall-off at small scales. This is similar to the behaviour found by Linden *et al.* (1994) in their concentration fluctuation spectrum.

The growth of kinetic energy shown in figure 2(d) gives another picture of the unfolding of the instability. There is a well-defined period of exponential growth even before $t = 2.5$ when diffusion still dominates. We find that the maximum growth rates decrease almost linearly with Ro. The fact that the decrease of the growth rate with increasing Ro begins from the earliest moments suggests that we may be able to understand something about the effects of rotation, at least in the early phase, without recourse to turbulence theory. We pursue this idea in the next section.

4. Suppression of the growth of a single bubble

In an attempt to understand the role of rotation in suppressing the growth of the mixing zone, we have performed a series of simulations of the growth of a single isolated bubble for different values of Ro. Each simulation was initialised with a circularly symmetric perturbation which bent the isopycnals (equal density surfaces) slightly upward in the middle of the domain. Specifically, we added the following small-amplitude perturbation to the unperturbed scaled density θ in (2.1):

$$\theta' = a \exp((-x^2 - y^2)/b^2) \exp(-z^2/c^2) \qquad (4.1)$$

with $a = -0.025$, $b = 0.05$ and $c = 0.01$. These values were chosen through experimentation which showed that the proximity of the walls did not affect the growth of the
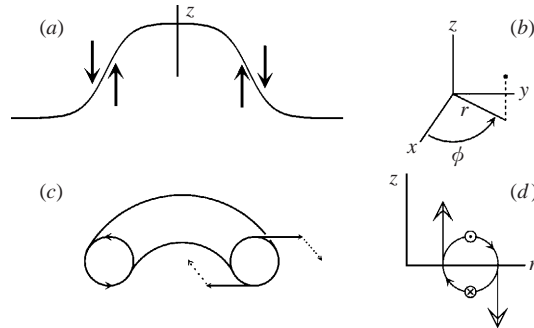
FIGURE 4. Schematic illustrating the effect of Coriolis force in the early evolution of a bubble. (*a*) A vertical cross-section illustrating the effect of the baroclinic torque exerted on the fluid due to the initial bending of an isopycnal. The arrows are the velocities induced by the action of gravity. This creates a vorticity component ω_ϕ around the interface in between each pair of arrows creating the vortex ring shown in (*c*), where a vertical cross-section is taken to reveal the flow structure. In (*c*) the extended solid arrows on the rightmost circle show the direction of flow induced by ω_ϕ. The dashed arrows, which represent flow directly into and out of the page, show the change in velocity induced by the Coriolis force. The application of this force to that secondary flow creates a flow directly counter to the original flow indicated by the solid arrows. (*d*) The forces acting to create the flow. The large circle is a vertical cross-section of the vortex ring. The large arrows represent the buoyancy forces. ⊙ and ⊗ indicate the Coriolis force out of and into the page respectively.

bubble. In figure 3, we show a comparison between the state of development for the resulting bubble at $t = 4$ for $Ro = \infty$ and $1/4$. The figures are vertical cross-sections (y, z-plane) through the centre of the bubbles. In addition to indicating the position of the middle of the density gradient (the $\theta = 0.5$ contour line), we also show contours of the x-component of the relative vorticity ω_x. In the case with no rotation (panel (*a*), $Ro = \infty$), by $t = 4$ a mushroom-like cap has formed on the advancing bubble and there is a strong vortex ring inside this cap. In contrast, in the case with rotation (panel (*b*), $Ro = 1/4$), at $t = 4$ a cap structure has not yet formed, and the vorticity field is much weaker. Clearly rotation slows the growth of the bubble. Note that, for each case shown, if we change the sign of the initial density perturbation, the result would be a descending 'bubble' but with the same shape as that shown in figure 3 and with vorticity of opposite sign. This is a symmetry of the Boussinesq equations, that is of the low-Atwood-number approximation.

To gain some insight into the role that rotation plays in slowing the advance of a single bubble, it is convenient to introduce cylindrical coordinates as in figure 4(*b*). The bubble grows from the initial circularly symmetric (ϕ-independent) perturbation of the iso-density surface shown in figure 4(*a*). Note that there is a gradient $\partial\rho/\partial r$ not present in the unperturbed system. The arrows indicate the velocities induced by the action of gravity or, in other words, the flow induced by the baroclinic torque. This torque creates $\omega_\phi > 0$ in between the opposing arrows, which is the start of the formation of the vortex ring shown in (*c*). A vertical cross-section is taken through the centre of the ring to better reveal the flow structure. The small arrows on the leftmost circle, and the extended solid arrows on the rightmost circle show the direction of the flow induced by ω_ϕ. Once there is a horizontal flow component, the Coriolis force will act, and its effect will be to turn horizontal velocities to the right of their instantaneous direction. For the upper/lower arrow on the rightmost circle this means this flow is turned out/in from the plane of the figure as we have indicated with the dashed arrows. This secondary velocity field constitutes a new component of vorticity

$\omega_r > 0$, which never occurs in the $Ro = \infty$ case. The Coriolis force continues to bend the flow 'to the right'. If we now imagine that the dashed arrows are bent to their right, we see that the Coriolis force induces a flow in a direction directly opposite to that associated with the original vortex. Thus the Coriolis force tends to create a vorticity component ω_ϕ of opposite sign to that of the ω_ϕ initially created by the density disturbance. Figure 4(*d*) displays the forces acting to create the flow shown in (*c*).

One can see this effect in the Boussinesq equations most easily when they are written in cylindrical coordinates. There is a simplification since the fields for the single bubble problem are independent of the angle ϕ for all time. Thus we can write the evolution equations for the vorticity field in the inviscid non-diffusive case as

$$\frac{\partial \omega_r}{\partial t} = f\frac{\partial u_r}{\partial z} + (\nabla \times (\boldsymbol{u} \times \boldsymbol{\omega}))_r, \tag{4.2}$$

$$\frac{\partial \omega_\phi}{\partial t} = -f\omega_r + \frac{g}{\rho_0}\frac{\partial \rho}{\partial r} + (\nabla \times (\boldsymbol{u} \times \boldsymbol{\omega}))_\phi, \tag{4.3}$$

$$\frac{\partial \omega_z}{\partial t} = f\frac{\partial u_z}{\partial z} + (\nabla \times (\boldsymbol{u} \times \boldsymbol{\omega}))_z, \tag{4.4}$$

$$\frac{\partial \rho}{\partial t} = -u_r\frac{\partial \rho}{\partial r} - u_z\frac{\partial \rho}{\partial z}, \tag{4.5}$$

$$\frac{1}{r}\frac{\partial ru_r}{\partial r} = -\frac{\partial u_z}{\partial z}, \tag{4.6}$$

where $\rho_0 = (\rho_1 + \rho_2)/2$ (the average density). The last equation expresses the vanishing of the divergence and has been used to obtain (4.4). Also we have used the ϕ-independence to substitute ω_r for $-\partial u_\phi/\partial z$ in (4.3).

For the moment, let us ignore the effect of the nonlinear terms $\nabla \times (\boldsymbol{u} \times \boldsymbol{\omega})$ and $u_r\partial\rho/\partial r$ which are of at least quadratic order in an amplitude expansion. Now the effects described with the schematic diagram (figure 4) can be seen in these equations. At $t = 0$, the only non-vanishing term on the right-hand side of the evolution equations is $(g/\rho_0)\partial\rho/\partial r$ in (4.3). This term is the initial source of ω_ϕ. Once generated, this vorticity component induces positive $\partial u_r/\partial z$ as explained above, and that field in turn generates positive ω_r through (4.2). This ω_r then diminishes the growth of ω_ϕ as seen in (4.3). If we look at the fields early in the evolution of the single bubble, we can follow the emergence of each of these fields and their effects. In figure 5 we present an r, z cross-section of these fields at $t = 0.5$. Since the flow is circularly symmetric, an r, z cross-section is representative of the entire ring.

Our analysis can be made more precise with a small time expansion. We develop each of the velocities and the density field in a Taylor series in time. These are substituted into the evolution equations and orders in time are matched. In this way we find that ρ, ω_r and ω_z are even in time, while ω_ϕ is odd, at least up to order t^4. For example, we find

$$\omega_\phi = \omega_\phi^{(1)}t + \omega_\phi^{(3)}t^3/3! + O(t^4), \quad \rho = \rho^{(0)} + \rho^{(2)}t^2/2! + O(t^4), \tag{4.7}$$

where

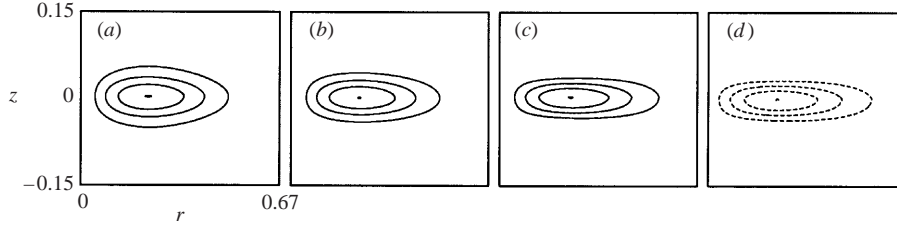$$\omega_\phi^{(1)} = \frac{g}{\rho_o}\frac{\partial \rho^{(0)}}{\partial r}, \tag{4.8}$$

FIGURE 5. Contour plots with $Ro = 1/4$ at $t = 0.5$ of the fields most relevant to the discussion of the early evolution of the single bubble in an r, z cross-section. (*a*) ω_ϕ; (*b*) $g\partial\rho/\partial r$, the initial source of ω_ϕ; (*c*) $f\partial u_r/\partial z$, a field induced by ω_ϕ and in turn a source of ω_r; (*d*) $-f\omega_r$, the Coriolis term retarding the growth of ω_ϕ (see text). The contour increments are: (*a*) 0.0096, (*b*) 0.038, (*c*) 0.022 and (*d*) 0.026. The zero contour is not drawn. Dashed contours represent negative values. Only a small portion of the computational domain is represented.

and

$$\omega_\phi^{(3)} = -f^2\frac{\partial u_r^{(1)}}{\partial z} - \frac{g}{\rho_o}\frac{\partial}{\partial r}\left(u_r^{(1)}\frac{\partial\rho^{(0)}}{\partial r} + u_z^{(1)}\frac{\partial\rho^{(0)}}{\partial z}\right) - 2\frac{\partial}{\partial z}\left(u_z^{(1)}\omega_\phi^{(1)}\right) - 2\frac{\partial}{\partial r}\left(u_r^{(1)}\omega_\phi^{(1)}\right). \quad (4.9)$$

Note that here we have now explicitly included the effects of the nonlinear terms that were ignored in our previous discussion. The velocity fields $u_r^{(1)}$ and $u_z^{(1)}$ are those induced by the vorticity $\omega_\phi^{(1)}$. With the aid of the Green function for this problem these velocities could be written as a linear functional of $\omega_\phi^{(1)}$. However, introducing Green's function is a complication that is not necessary for present purposes. Here it is sufficient to note that there is no dependence on f in any of the $O(t)$-fields since they depend only on the initial density perturbation. Thus, up to $O(t^3)$ the effect of the Coriolis force on ω_ϕ appears only in the first term on the right-hand side of (4.9). The reason why in this term f appears raised to the second power is related to the fact that it requires both the generation of a u_ϕ-component of velocity and then a secondary u_r-component to affect the field ω_ϕ as discussed above. The sign of this term can be deduced from the schematic diagram of the vortex ring in figure 4. There the ring is drawn with the direction of flow appropriate for $\omega_\phi > 0$, and it illustrates that $\partial u_r/\partial z > 0$ in that case. Hence, the sign of the f^2-term in (4.9) is opposite to that of $\omega_\phi^{(1)}$.

We can make further progress by assuming that the amplitude of the perturbation is small, so that terms quadratic in amplitude in (4.9) can be ignored. Let us write the density perturbation as $\rho'(r, z)$ (i.e. $\rho = \bar{\rho} + \rho'$). Since $\omega_\phi^{(1)}$ depends on the density only through the r-derivative, it is linear in ρ'. Consequently, $u_r^{(1)}$ and $u_z^{(1)}$ are also at lowest order linear in ρ'. By examining all terms in (4.9), we find all but two are second order in ρ', and can thus be neglected if the ratio $\rho'/\bar{\rho}$ is sufficiently small. This leaves

$$\omega_\phi^{(3)} = -f^2\frac{\partial u_r^{(1)}}{\partial z} + N^2\frac{\partial u_z^{(1)}}{\partial r}, \quad (4.10)$$

where we have used the traditional notation

$$N^2 = -\frac{g}{\rho_o}\frac{\partial\bar{\rho}}{\partial z}, \quad (4.11)$$

but must add the caution that in this case N^2 is negative (i.e. the Brunt–Väisällä frequency is imaginary). To make further progress, we could take the initial radius of the bubble to be sufficiently large that, in a vertical cross-section, the flow near the
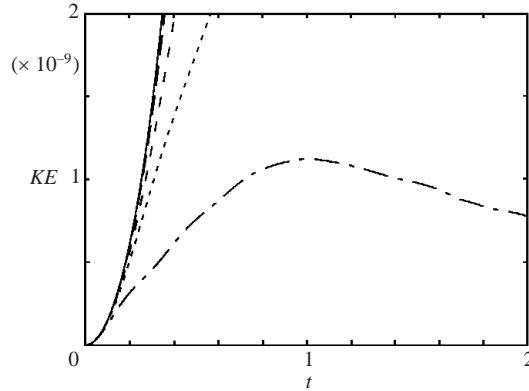
FIGURE 6. Graphs of the growth of the kinetic energy for a single bubble. Solid line, $Ro = \infty$; long dashed, $Ro = 1/4$; dashed, $Ro = 1/8$; short dashed, $Ro = 1/12$; chain-dashed, $Ro = 1/24$.

centre of the core of the initial vortex ring would be nearly two-dimensional and the two-dimensional divergence would nearly vanish. Furthermore, with this assumption we can ignore the self-advection of the ring which diminishes with ring radius. Under these conditions, for flow near the centre of the core, we can write

$$\partial u_r^{(1)}/\partial z \approx -\partial u_z^{(1)}/\partial r \approx \omega_\phi^{(1)}/2. \tag{4.12}$$

Finally, we have

$$\omega_\phi^{(3)} = -(N^2 + f^2)\omega_\phi^{(1)}/2. \tag{4.13}$$

Thus the growth of the instability due to negative N^2 is diminished by rotation. It is interesting to note that this solution to $O(t^3)$ is equivalent to the solution to the simple wave equation

$$\frac{\partial^2 \omega_\phi}{\partial t^2} = -\tfrac{1}{2}(N^2 + f^2)\omega_\phi. \tag{4.14}$$

This suggests that the growth rate for the early evolution could be obtained directly from the dispersion relation for internal waves in a uniformly stratified medium (Gill 1982):

$$\sigma^2 = \frac{N^2 + f^2(k_z/k_h)^2}{1 + (k_z/k_h)^2}, \tag{4.15}$$

where k_z and k_h are the vertical and horizontal wavenumbers of the disturbance, and σ the frequency. In our case the 'disturbance' is the vortex ring and we have assumed that the core is circular which is equivalent to taking $k_z = k_h$. Substituting this into the dispersion relation gives the same result as in (4.14).

For the cases presented here, non-dimensionally $N_{\max}^2 = -80$. Figure 6 shows the early evolution of the kinetic energy of the flow for a single bubble with non-dimensional $f = 0$, 4, 8, 12 and 24 (non-dimensionally $Ro = 1/f$). Note that the early growth for the large Rossby number cases (small f) is nearly quadratic in time. This includes the self-advection of the vortex ring. If ω_ϕ grows as t then there is, in addition to the circular motion about the core, a self-advection velocity u_z which is inversely proportional to the radius of the ring (cf. Verzicco *et al.* 1996). This part of the velocity has been neglected in our large ring approximation (4.12) leading to (4.13). In any case, the theory suggests a crossover in behaviour near $f = \sqrt{80} \approx 8.9$ ($Ro \approx 0.11$). From figure 6, it appears that there is indeed a change in behaviour

as f increases, with cross-over occurring between $Ro = 1/12$ and $1/24$. At later times, the perturbation kinetic energy for the $Ro = 1/24$ case continues to decay while the density gradient diffuses. Thus the instability is completely suppressed. For simulations with random initial density perturbations as in figure 1, we found complete suppression with $Ro = 1/48$.

Although helpful in providing a mechanistic understanding of the initiation of the instability, (4.13) includes neither viscosity nor diffusion. Recalling Hide's (1956) work, it appears that the presence of rotation and viscosity alone cannot completely suppress the instability. Here we have found that rotation with viscosity and diffusion, at least in the Boussinesq approximation, can completely suppress RTI.

REFERENCES

GILL, A. E. 1982 *Atmosphere-Ocean Dynamics*. Academic.

HIDE, R. 1956 The character of the equilibrium of a heavy, viscous incompressible rotating fluid of variable density. II. Two special cases. *Q. J. Mech. Appl. Maths* **9**, 22–34.

LINDEN, P. F., REDONDO, J. M. & YOUNGS, D. L. 1994 Molecular mixing in Rayleigh-Taylor instability. *J. Fluid Mech.* **265**, 97–124.

ORLANDI, P. 2000 *Fluid Flow Phenomena: A Numerical Toolkit*. Kluwer.

SEN, S. & STORER, R. G. 1997 Suppression of Rayleigh-Taylor instability by flow curvature. *Phys. Plasmas* **4**, 3731–3733.

VERZICCO, R., ORLANDI, P., EISENGA, A. H. M., VAN HEIJST, G. J. F. & CARNEVALE, G. F. 1996. Dynamics of a vortex ring in a rotating fluid. *J. Fluid Mech.* **317**, 215–239.

ZABUSKY, N. J. 1999 Vortex paradigm for accelerated inhomogeneous flows: visiometrics for the Rayleigh-Taylor and Richtmyer-Meshkov environments. *Annu. Rev. Fluid Mech.* **31**, 495–536.